

## Behavior of SFRC interior beam-column joints under cyclic loading

Noor Ayaad Khalaf and Musab Aied Qissab\*

*Department of Civil Engineering, Al-Nahrain University, Baghdad, Iraq*

*(Received April 23, 2020, Revised June 5, 2020, Accepted June 9, 2020)*

**Abstract.** In this paper, the behavior of interior steel fiber reinforced concrete beam – column joints (BCJs) under cyclic loading is investigated. An experimental program including tests on twelve reinforced concrete (BCJs) specimens under cyclic loading was carried out. The test specimens are divided into two groups having different geometry: group (G1) (symmetrical BCJs specimens) and group (G2) (nonsymmetrical BCJs specimens). The parameters considered in this study are the steel fibers (SFs) content by volume of concrete ( $V_f$ ), the spacing of shear reinforcement at the joint region, and the area of longitudinal flexural reinforcement. Test results show that the addition of 0.5% SFs with stirrups spacing  $S=S_{max}$  has effectively enhanced the overall performance of BCJs with respect to energy dissipation, ductility ratio, spreading and width of cracks. The failure of specimens is governed mainly by the formation of a plastic hinge at the face column and outside the beam-column junction. Secondary shear cracks were also observed in the beam-column junctions.

**Keywords:** interior beam – column joints; steel fibers; ductility ratio; energy dissipation capacity; cyclic loading

### 1. Introduction

Failure of many structures took place in last decades due to the hurricane, floods, earthquakes and explosions. These types of events impose severe loadings on building's structure and may cause failure at critical members especially at beam-column joints (Nimse *et al.* 2014) (Xilin *et al.* 2012) (Zhou and Zhang 2014). Joints are critical members in any structure. If these members are not properly designed to resist and redistribute the additional loads, structural failure may take place. Seismic force is a type in which horizontal and vertical force components its magnitudes are very much higher at the BCJs. These forces which are acting at the junction might interrupt the shear strength of the member (UFC 4-023-03 DoD 2016). Column shear failure is the main cause of building failure during earthquakes. The other local failure takes place due to gravity loads which transfer to the neighboring members in the structure; as a result, a substantial part of the structure may damage or removed (Moehle *et al.* 2008). These failure scenarios require a certain level of ductility and continuity in BCJs to redistribute vertical loads (Kang and Tan 2015).

BCJs have been identified potentially as one of the important components of reinforced concrete moment resisting frames subjected to seismic actions (Kim and La Fave 2009). The specific

---

\*Corresponding author, Assistant Professor, E-mail: [musabaq79@gmail.com](mailto:musabaq79@gmail.com)

structural properties termed as strength, stiffness and ductility need to be taken into consideration. For adequate ductility of the beam-column junction, the use of closely spaced hoops as transverse reinforcement was recommended in the ACI-ASCE committee report 352. However, due to congestion of reinforcement, casting of BCJs becomes difficult and leads to honeycombing in concrete at these joints (Kumar *et al.* 1991). In reinforced concrete frames this ductility is usually achieved by inelastic rotation of plastic hinges located in the beams, normally adjacent to the column faces (Beckingsale 1980). In general, failure in a BCJ may occur in one of the following ways (Kumar 1988): formation of the plastic hinge in beam portion near the beam-column interface, the formation of a plastic hinge in column portion near the joint core and formation of diagonal crack at the joint region. The contributions of the two mechanisms to shear transfer vary in proportion depending on the conditions of damage within the joint and adjacent framing members (Paulay *et al.* 1978). Finally, bond deterioration by low quantities of longitudinal reinforcement in the web, failure can be due to yielding of longitudinal reinforcement leading to a sliding displacement, the force in a bar passing continuously through the joint changes from compression to tension causing a push-pull effect with the distribution of bond stress.

To resist concrete cracking, different types of fibers such as steel fibers (SFs) were used to improve the ductility and energy dissipation at the BCJs under reversed cyclic loading (Ganesh and Prabavathy 2015). In the last decades, the implementation of steel fiber reinforced concrete (SFRC) has significantly increased all over the world as an effective alternative to conventional reinforcement (reinforcing bars or welded wire mesh). A diffused steel fiber reinforcement may improve the structural behavior and on the other hand, SFRC is capable of sustaining considerable loads even at deflections considerably in excess of the fracture deflection of the ordinary reinforced concrete subjected to the reversed cyclic loading (Sorelli *et al.* 2006). Steel fibers can be used with different parameters such as aspect ratio ( $l/d$ ) and geometrical shape which can be added to the concrete mixture as a fraction of the total volume of mixture ( $V_f$ ). SFs can be classified according to the production process, material and shape (ACI 544.1R-96, 2002). In fact, a linear elastic approach cannot properly take into account the beneficial effects of fiber reinforcement which become effective only after cracking of the concrete matrix when SFRC behavior is significantly nonlinear. Fibers become active after cracking (not visible micro-cracks) of the concrete matrix. Because fibers of different size become efficient at different stages of the cracking process. However, a hybrid combination of short and long steel fibers may enhance the concrete toughness at small crack opening displacements (Banthia *et al.* 2000) (Sorelli 2000) (Sorelli 2005). Recent research conducted by Jianan *et al.* (2019), Oinam *et al.* (2019), Sarmiento *et al.* (2019), and Nguyen *et al.* (2020) also confirmed the positive impact of the addition of steel fiber on the post-cracking behavior of concrete.

Current design recommendations for RC/ BCJs in the earthquake-resistant construction given by (ACI-ASCE Committee 352, 2002) focus on three main aspects: 1) confinement requirements; 2) evaluation of shear strength; and 3) anchorage of beam and column bars passing through the connection. Additionally, a strong column-weak beam behavior must be ensured, and frame members or regions expected to experience large reversed inelastic deformations must be properly detailed to ensure sufficient displacement capacity during earthquakes.

Sara *et al.* (2015) tested two half-scaled down roof interior BCJs under quasi-static cyclic loading. One of these specimens had wide beams on all four sides of the joint (RIWBC) and the other had conventional beams (RICBC). Results showed that the specimens' deformation capacity and the strength don't degrade up to a drift level of 4% and 3% in specimens RIWBC and RICBC respectively. The energy dissipation capacity of specimen RIWBC was similar to that for RICBC

specimen. Moreover, the capacity and secant stiffness of the RIWBC specimen was lower than RICBC ones.

Romanbabu *et al.* (2013) investigated the behavior of three scaled-down BCJs with a scale factor of (1/3) and subjected to cyclic loading. All specimens were cast by using plain RC, SFRC and had been detailed according to the provisions of IS: 13920 incorporating similitude requirements. Three specimens had been considered, namely RCBC (reinforced concrete beam-column as control specimen), SFBC (steel fiber beam-column) and PFBC (polypropylene fiber beam-column). The ultimate load carrying capacity was increased by 17.37% and 8.95% for SFBC and PFBC specimens respectively. The ductility of SFBC and PFBC specimens was increased by 99.4% and 105% respectively with respect to specimen RCBC.

Keerthana and Reddy (2014) carried out an experimental program to study the behavior of reinforced concrete BCJs with steel fibers like crimped hook end and had been used with different volume fractions and aspect ratios. For each specimen, the column was subjected to axial force while the beams were subjected to cyclic loading under displacement control. It was observed that the use of hybrid SFs increases the energy dissipation by 28.3% for non-ductile and 31.6% for ductile reinforced concrete BCJ strengthened by hybrid SFs. Sohailuddin and Shaikhm (2013) carried out a finite element modeling of four type of exterior BCJs by using (ANSYS11.0). The BCJ specimens were subjected to the same reverse cyclic loading to simulate earthquake loading on structures. The comparison showed a better performance of the BCJ when it was provided with cross bars of 8 mm in beam region.

Liang *et al.* (2016) investigated the seismic behavior of reinforced concrete interior beam column joints with polyvinyl alcohol (PVA) fibers under reversed cyclic load experimentally and numerically. It was observed that the seismic performance of (BCJs) was improved with the addition of (PVA) fibers with respect to ductility and energy dissipation capacity. The OpenSees software was used for the numerical analysis and good agreement was obtained with the test results.

According to the abovementioned review of previous works, there is a limited number of research works that deal with the behavior of SFs reinforced concrete BCJs under cyclic loading. Furthermore, the response of interior SFs reinforced concrete BCJs under gravity cyclic loads is not yet well investigated. Interior beam-column joints are often subjected to vertical or gravity severe cyclic loading when an interior column is removed or become out of service as a result of a strong earthquake or explosion. The capability of a beam-column assembly to sustain cyclic gravity loading after a column removal scenario is of great importance for collapse prevention performance level under extreme events. The addition of steel fiber to concrete can significantly increase the ductility and the post-crack energy dissipation capacity of concrete which, in turn, can decrease the probability of complete collapse of reinforced concrete buildings subjected to column removal scenarios under extreme events. Accordingly, the main objective of this paper is to investigate the hysteresis response of interior BCJs with steel fibers (SFs) considering different fiber contents subjected to vertical cyclic loading as a simulation of column removal scenario. BCJs with hooked-ended shape SFs were tested under reversed gravity cyclic loading and the main parameters investigated were: number of loading cycles to failure, flexural ductility ratio, energy dissipation capacity, cracking pattern at failure and residual displacement.

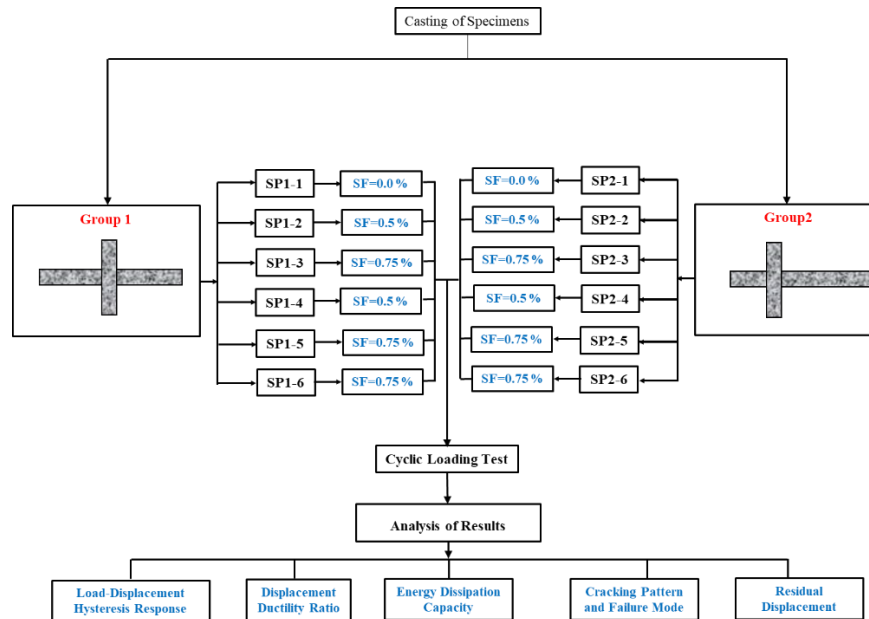


Fig. 1 Flowchart of the experimental program

## 2. Experimental program



### 2.1 Test specimens

In order to study the effect of test parameters on the cyclic behavior of BCJs with SFRC, twelve specimens were tested. In addition to the six symmetrical BCJs specimens, additional six nonsymmetrical BCJs were considered to increase the possibility of shear failure of the beam-column junction as a critical case. Accordingly, test specimens are divided into two groups: group (G1) and group (G2). The groups were tested under reversed vertical cyclic loading. Each group comprises six specimens and had geometry and properties as shown in Table 1. All specimens were designed to fail in flexural failure mode caused by either bond of flexural reinforcement of the beam or yielding of longitudinal reinforcement leading to a sliding displacement. Two specimens, SP1-1 and SP2-1, were cast with normal concrete without SFs as reference specimens to the group (G1) and group (G2) respectively. The flowchart of the experimental program is shown in Fig. 1 while the geometry and dimensions of the test specimens are shown in Fig. 2. The reinforcement details of the specimens are shown in Figs. 3(a) and 3(b). Fig. 4 shows the casting process of the test specimens while Fig. 5 shows the test specimens ready for testing.

### 2.2 Materials

Ordinary Portland cement, river sand passing through (4.75) mm sieves and a coarse aggregate size of (12) mm were used. Portable water was used for both mixing and curing. M35 grade concrete was adopted in this study. Water/cement ratio was (0.43) and the mix proportions were 1 (cement): 2.02 (sand): 2.5 (gravel). The quantity of cement used was (420 kg/m<sup>3</sup>).

Table 1 Properties and reinforcement details of test specimens

Group No.	Specimen designation	Geometry Type	Ratio of steel fibers% $V_f$	Reinforcement detail No.
1	SP1-1		0.00	(1)
	SP1-2		0.50	(1)
	SP1-3		0.75	(1)
	SP1-4		0.50	(2)
	SP1-5		0.75	(2)
	SP1-6		0.75	(3)
2	SP2-1		0.00	(4)
	SP2-2		0.50	(4)
	SP2-3		0.75	(4)
	SP2-4		0.50	(5)
	SP2-5		0.75	(5)
	SP2-6		0.75	(6)

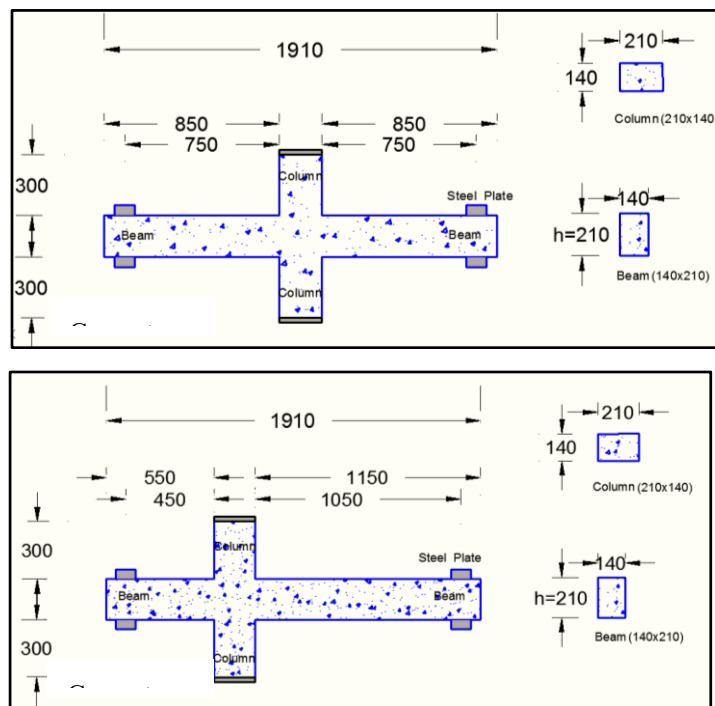
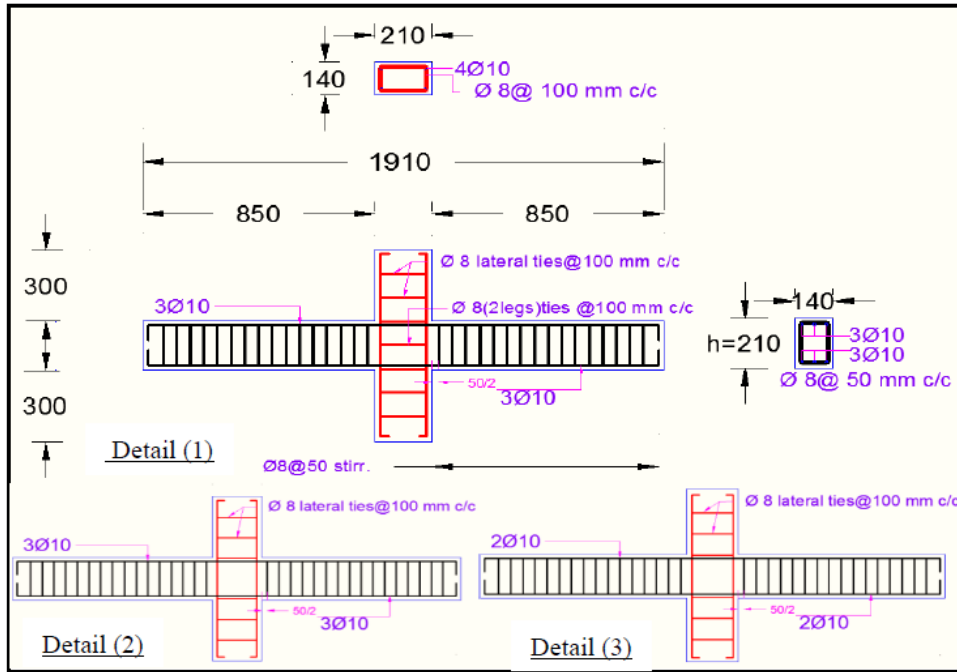
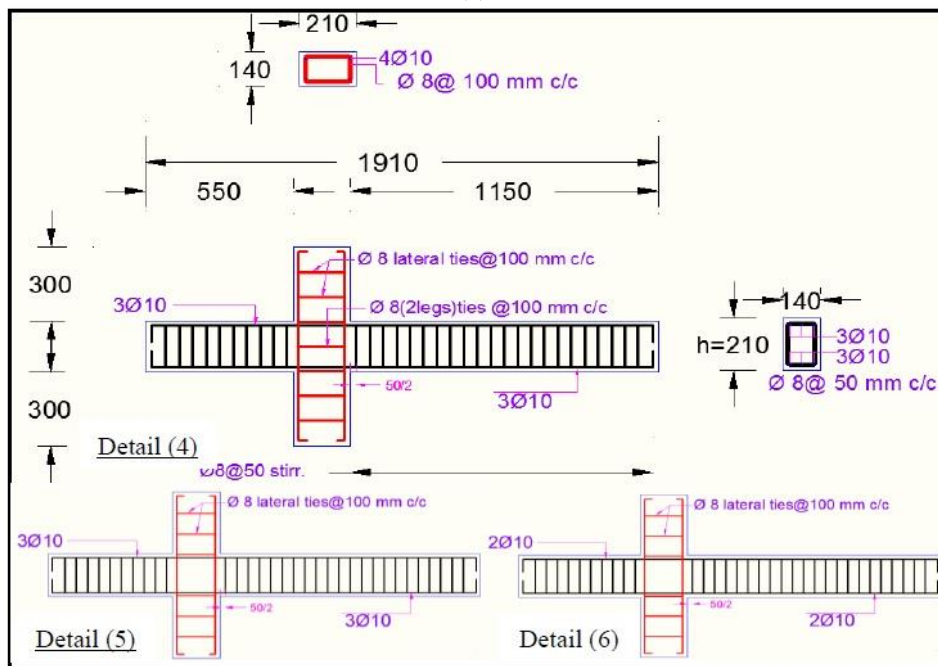


Fig. 2 Geometry and dimensions for specimens of group (G1) and group (G2) (All dimensions in mm)



(a)



(b)

Fig. 3 (a) Specimen dimensions and reinforcement details (All dimensions in mm) and (b) Specimen dimensions and reinforcement details (All dimensions in mm)

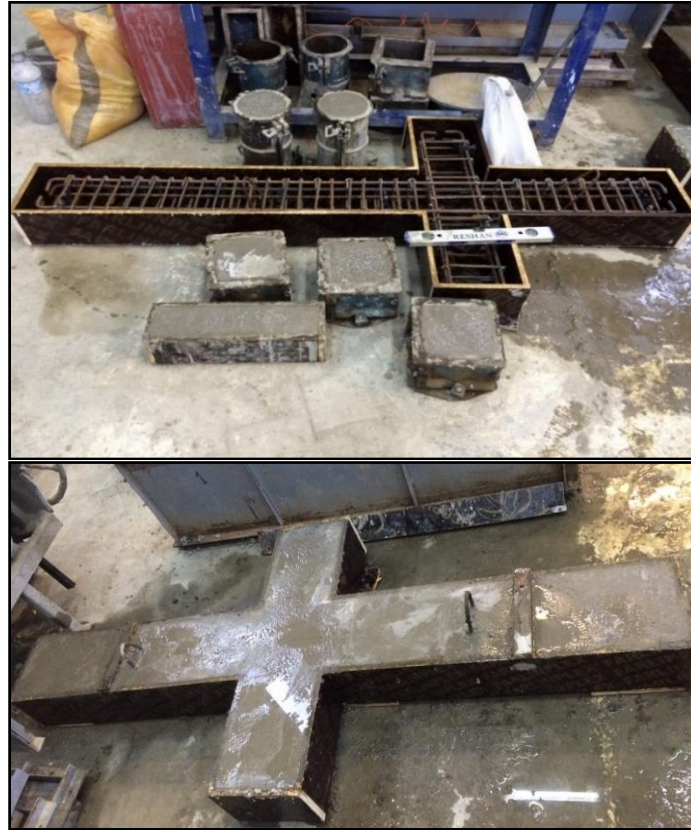


Fig. 4 Casting of test specimens

Table 2 Physical properties of steel fibers

Property	Specifications
Source	Turkey
Type	Hook ended shape
Density	7480 kg/m <sup>3</sup>
Tensile strength $f_y$	Min 1100 MPa
Modulus of Elasticity	$200 \times 10^3$ MPa
average length ( $l_f$ )	50 mm
Nominal diameter ( $d_f$ )	0.75 mm
Aspect ratio ( $l_f/d_f$ )	67



Fig. 5 Test specimens ready for testing



Fig. 6 Discrete steel fibers

Sika ViscoCrete-5930 (2010) which is a high-performance superplasticizer (SP) concrete admixture was used as a surfactant in this study. The SFs used have an aspect ratio ( $l/d$ ) of 67 with hooked ends, which were uniformly distributed in concrete mix. The SFs were zinc galvanized wires with silver color as shown in Fig. 6. The physical properties of SFs provided by the manufacturer are given in Table 2. The ratios of (SP) and SFs used in this study are given in Table 3.





Fig. 7 Sampling and testing of fresh concrete

Table 3 The ratios of SP and SFs used in this study

Mix Symbol	Superplasticizer % by weight of cement	Specimen
Reference mixture	0.35	SP1-1, SP2-1
Mixture with SFs 0.5%	0.55	SP1-2, SP1-4, SP2-2 and SP2-4
Mixture with SFs 0.75%	0.65	SP1-3, SP1-5, SP1-6, SP2-3, SP2-5 and SP2-6

### 2.3 Mixture design and proportions

The concrete mixture for the reference BCJ specimens was designed as normal weight concrete according to British Mix Design Method BS 5328: Part 2: (1997). This mixture was designed to obtain the target design strength of (35 MPa) and a slump of (25-110) mm. The same mix proportions were used for specimens with SFs, but with different ratios of superplasticizer (SP). The materials content and steel fiber ratio are presented in Table 3. Fig. 7 shows the fresh concrete testing and sampling.

### 2.4 Test procedure

The specimens were tested as simply supported at the ends over an effective span of (1910 mm). A hydraulic testing machine with a capacity of (1000 kN) was used to test all specimens under

monotonic or cycle load up to failure. The test setup was composed of two major parts which are the supporting and loading systems. The two supporting ends of the specimens were fixed against vertical movements using a rigid steel assembly attached to two strong pairs of steel shafts located at the center of the beam and attached to the testing rig by means of slotted steel connection as shown in Fig. 8. The specimens were subjected to cyclic transverse displacement-controlled vertical loads as schematically shown in Fig. 9 and the loading history applied is shown in Fig. 10.

### 3. Results and discussion

#### 3.1 Mechanical properties of concrete

Compressive strength, splitting tensile strength, and flexural strength tests were carried out on concrete specimens. The compressive strength test was conducted according to BS 1881: part 116:1983 (1989) specifications. This test was conducted on  $(150 \times 150 \times 150)$  mm cubes. Cylindrical specimens with dimensions (150 mm dia.  $\times$  300 mm height) were used for splitting tensile strength



Fig. 8 The supporting system, hydraulic jacks, and the test setup

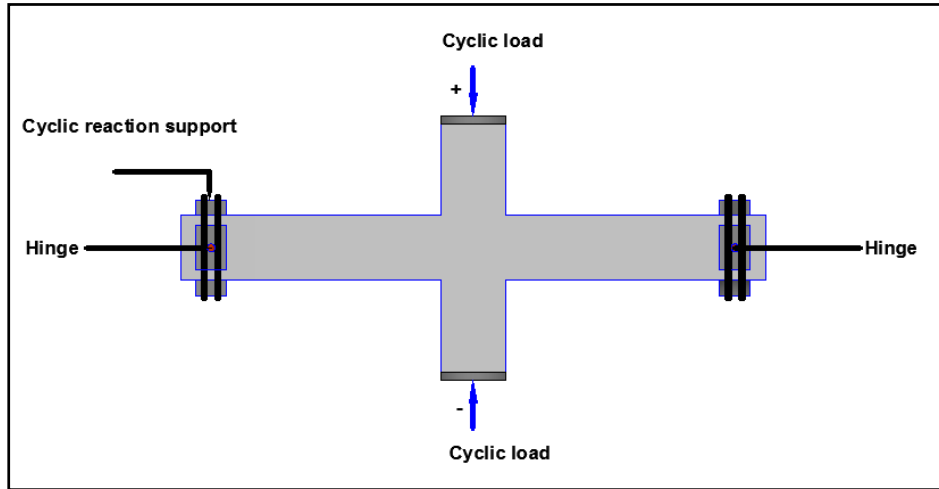


Fig. 9 Schematic diagram of the test setup

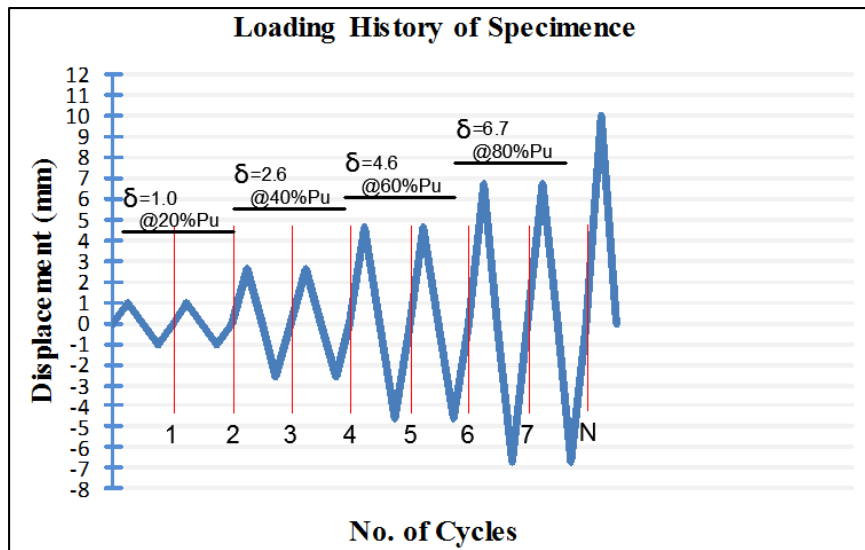


Fig. 10 Applied loading history

test in accordance to the ASTM C496/C496M-04 (2004). On the other hand, the flexural strength test was carried out on concrete prisms of dimensions (100 × 100 × 400 mm) with a span of 300 mm which were cast according to ASTM C-78(2002) specifications. The obtained results confirmed that the SFs increased the ductility of concrete, and improved the compressive strength, splitting tensile strength, and the flexural strength of concrete. The transfer of the tensile forces to SFs effectively prevents the propagation of micro cracks and improves the mechanical properties of concrete. Test results of the mechanical properties of concrete are presented in Table 4. Failure pattern of concrete specimens for the three tests are shown in Figs. 11 and 12.

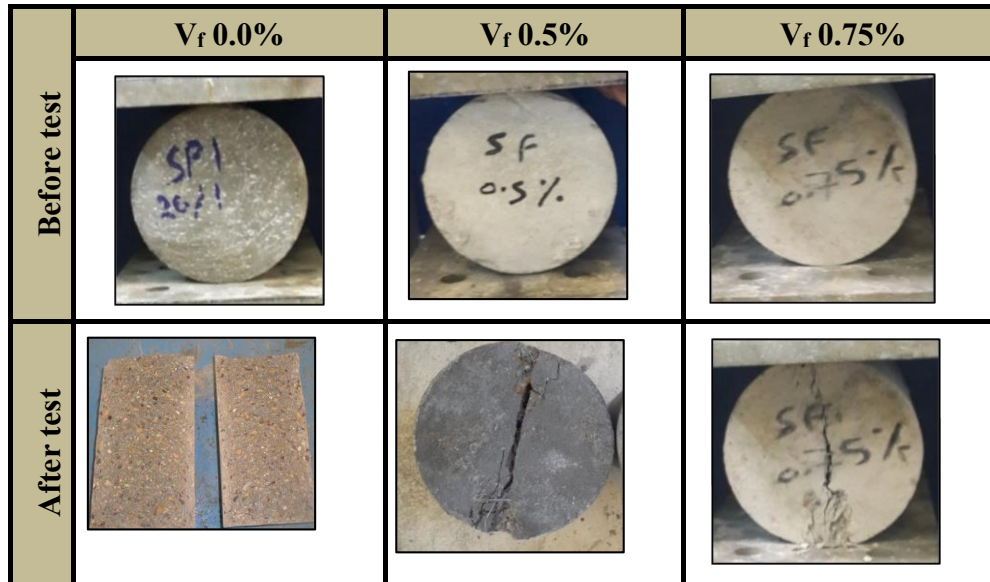


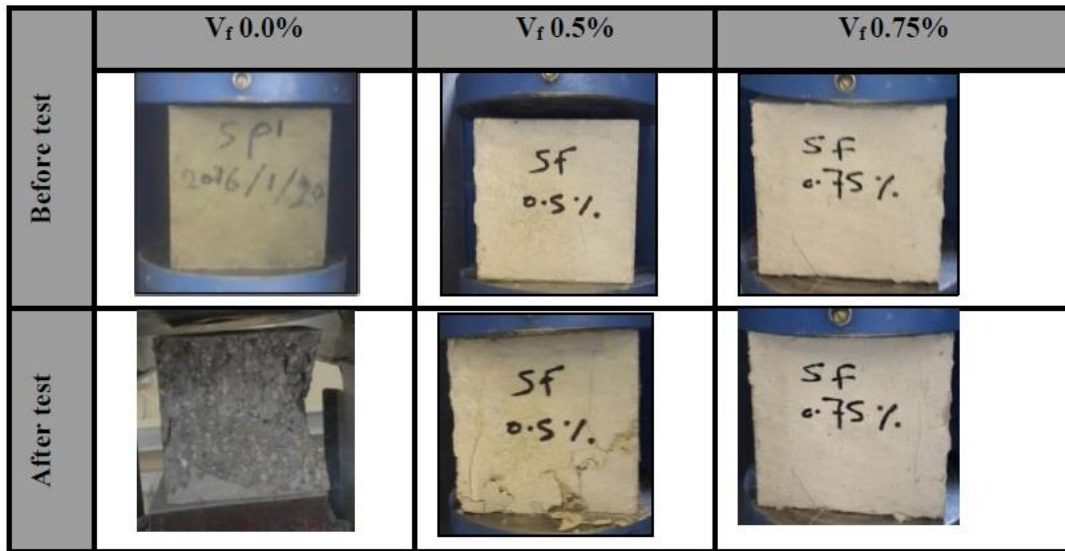
Fig. 11 Cracking pattern at failure of concrete specimens of splitting tensile strength test specimens

Table 4 Tests results for concrete specimens

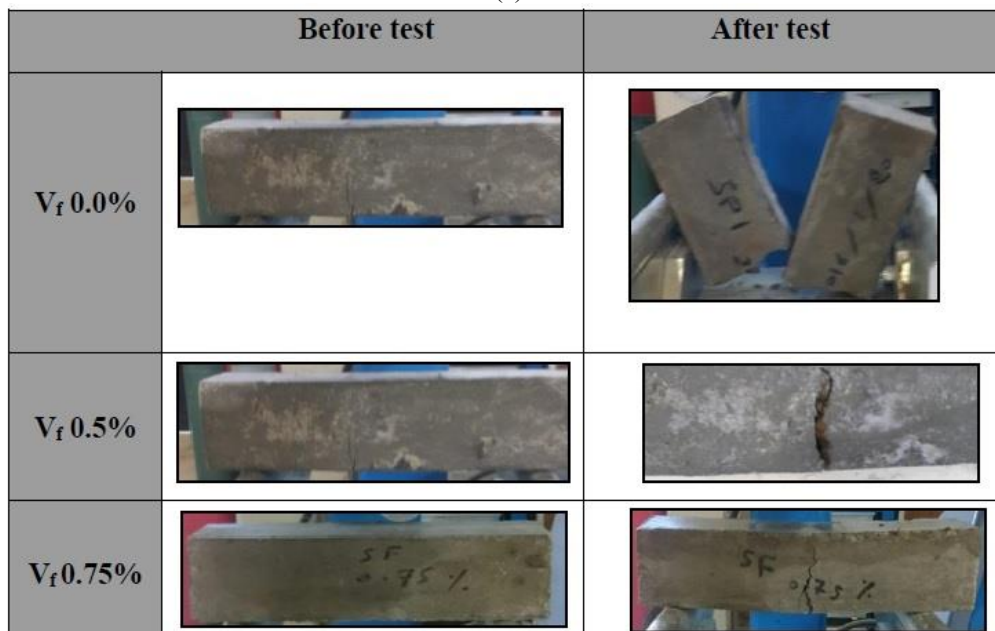
Specimen type	Compressive strength (N/mm <sup>2</sup> )	increase %	Splitting tensile strength (N/mm <sup>2</sup> )	increase %	Flexural strength (N/mm <sup>2</sup> )	increase %
(SP1-1, SP2-1) reference specimens	41.00	/	2.50	/	4.44	/
(SP1-2, SP2-2, SP1-4, SP2-4) Vf 0.5%	43.60	6.20	3.09	23.50	4.80	8.20
(SP1-3, SP2-3 SP1-5, SP2-5, SP1-6, SP2-6) Vf 0.75%	46.40	13.20	3.37	33.10	5.14	15.70

### 3.2 Results of tested beam specimens

In this study, the experimental results of the twelve BCJ specimens are presented. For each specimen, the main structural characteristics including the applied loading history, load carrying capacity, load - deflection behavior, flexural ductility factor, energy dissipation capacity, the cracking pattern, the failure mode and the response of specimens are presented and discussed. The transverse vertical load was monotonically applied in a displacement-controlled scheme as shown in Fig.10. The deflection was measured at the loading points automatically by the loading pistons which was a characteristic of the loading system used. For each specimen, load cycles were applied until complete failure is reached.



(a)



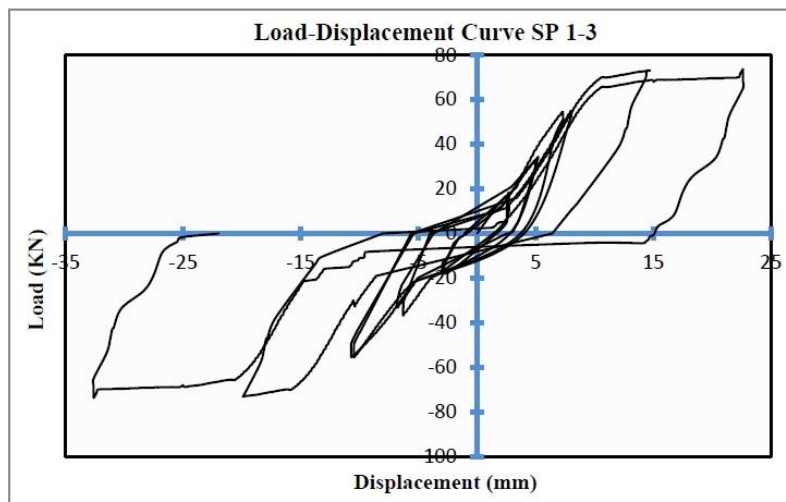
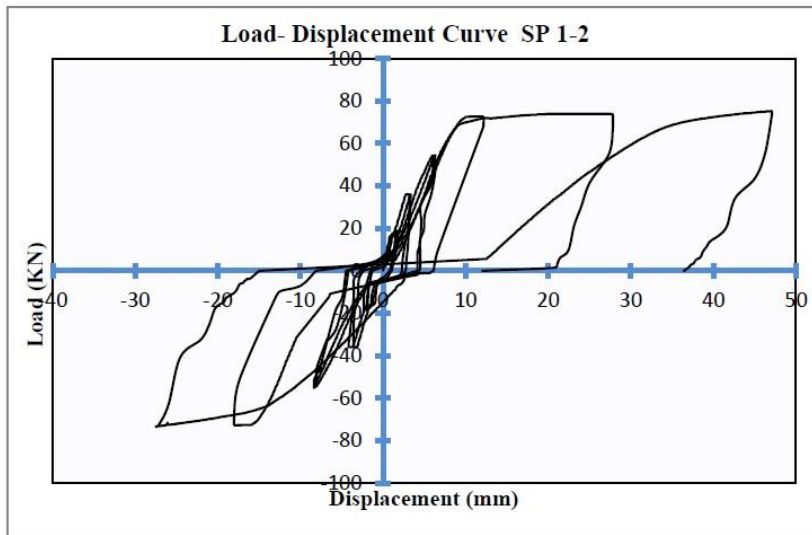
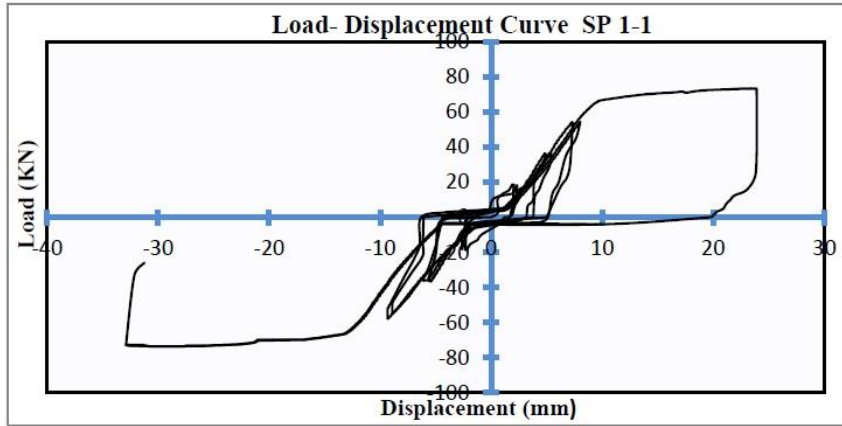
(b)

Fig. 12 Cracking pattern at failure of concrete specimens : (a) compressive strength test and (b) flexural strength test

### 3.2.1 Group (G1)

The test results for these specimens are summarized in Table 5. Specimens SP 1-1, SP 1-2, and SP 1-3 in this group have stirrups with spacing  $S=S_{max}$  at the joint region, while specimens SP 1-4, SP 1-5, and SP 1-6 have no stirrups. Fig. 13 shows the load-displacement hysteresis response for specimens of this group. Displacement ductility factor is defined as the ratio of the ultimate deflection at failure to the yield deflection which was obtained from the load – deflection envelope curve. The energy dissipation capacity was calculated as the area under the hysteresis loop of the load displacement curve for each loading cycle. For each cycle, the area under the load-displacement curve was calculated, approximately, by using the trapezoidal rule. The cumulative energy dissipation capacity of the specimen was obtained by summing the energy absorbed during each cycle. It can be seen from the presented results for specimens SP 1-2 and SP 1-3 that an increase in ductility and cumulative energy dissipation capacity was obtained with a better performance for specimen SP1-2. The range of increase is (20.3%-91%) and (16.0%-68.7%) for ductility and accumulative energy dissipation capacity respectively with respect to SP 1-1. On the other hand, for specimen SP 1-4, a reduction of (33.7%) and (25.8%) in ductility and accumulative energy dissipation was obtained respectively when compared to specimen SP1-2. The maximum load at failure for the aforementioned specimens is almost comparable with a slight increase for specimen SP1-2. This confirms that the use of (0.5%) SFs without stirrups in the joint region for specimen SP1-4 resulted in a lower confinement and crack bridging at the joint region in comparison to SP1-2. This is due to the fact that the presence of SFs reduces the number and width of cracks by bridging action between the two sides of a crack which in turns increases the ductility and capacity of the joint. In other words, it can be proposed that SFs can be used together with stirrups at a spacing of ( $S=S_{max}$ ) to improve significantly the response of BCJs under vertical cyclic loading. On the other hand, specimen SP 1-5 show an increase of (96%) and (60%) in ductility and a cumulative absorbed energy respectively with a higher failure load in comparison to specimen SP 1-1. The results confirmed that increasing the ratio of SFs without stirrups improved the concrete confinement, reduced the cracks width and increased the overall ductility and energy dissipation capacity. The results of this specimen confirm the possibility of elimination of steel stirrups in the joint region. For specimen SP 1-6, a longitudinal steel reinforcement of (2Ø10) instead of (3Ø10) top and bottom were used. Despite the reduction in longitudinal steel reinforcement for this specimen, a significant reduction in maximum load at failure and energy dissipation capacity with a slight reduction in ductility factor was observed in comparison to (SP 1-5). This is due to the fact that the reduction in longitudinal flexural steel caused a decrease in flexural capacity and the number of loading cycles of this specimen. However, an acceptable behavior was obtained for this specimen despite the prescribed observations. Table 5 also reports the average residual displacement (the mean value from positive and negative directions) for each specimen in this group. It is clear that the addition of SFs significantly increased the residual displacement as a result of increasing the ductility. The highest residual displacement was observed in specimen SP1-5. It can be confirmed that specimen SP1-2 shows a good performance among the rest with respect to maximum load at failure, ductility, energy dissipation and residual displacement.

The cracking pattern at failure for specimens of this group is shown in Fig. 14. An envelope curve for each test specimen is shown in Fig. 15. The results of the ductility factor and the cumulative energy dissipation capacity for all test specimens are shown in a bar chart in Figs. 16 and 17 respectively.



Continued-

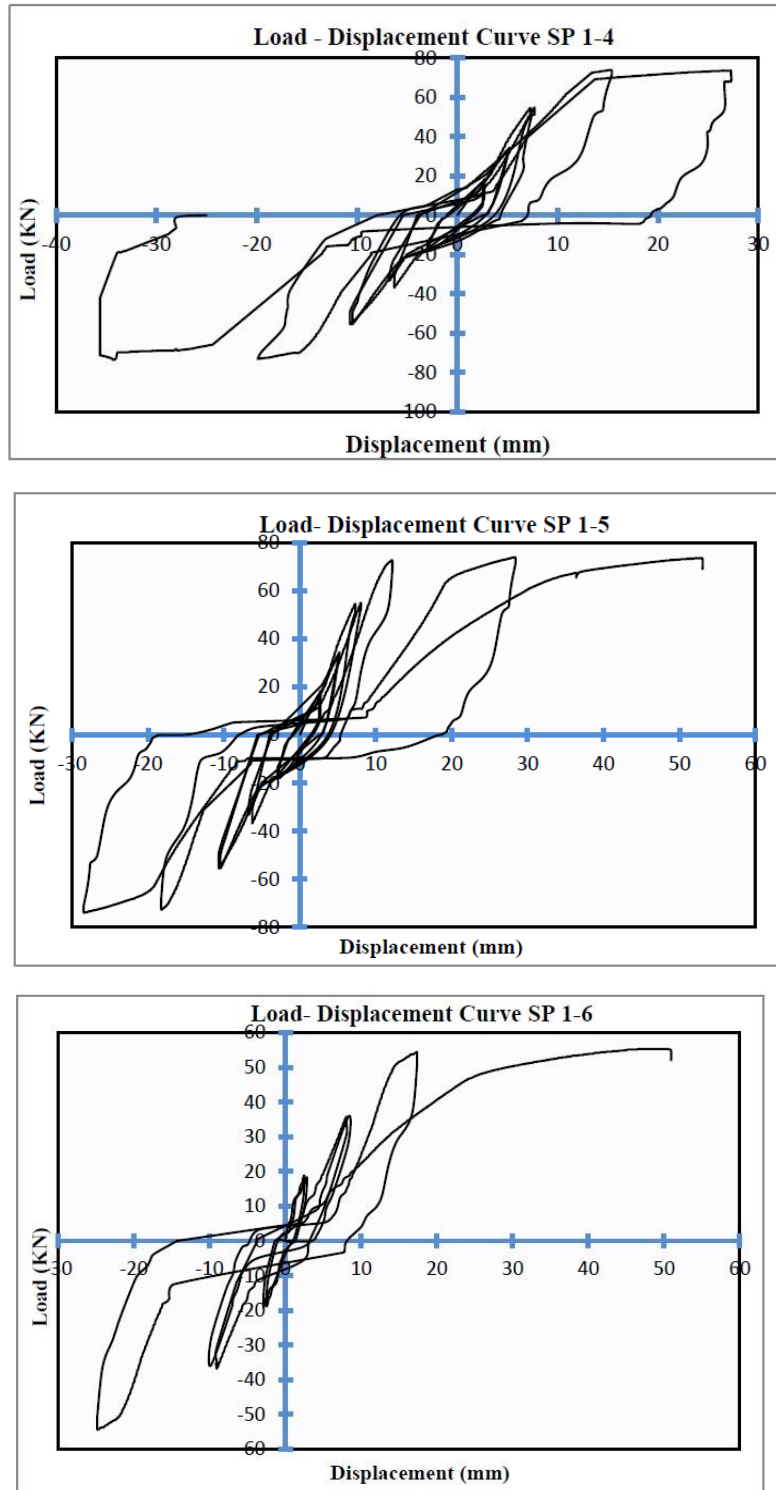


Fig. 13 Load- deflection hysteresis curves of test specimens of group (G1)



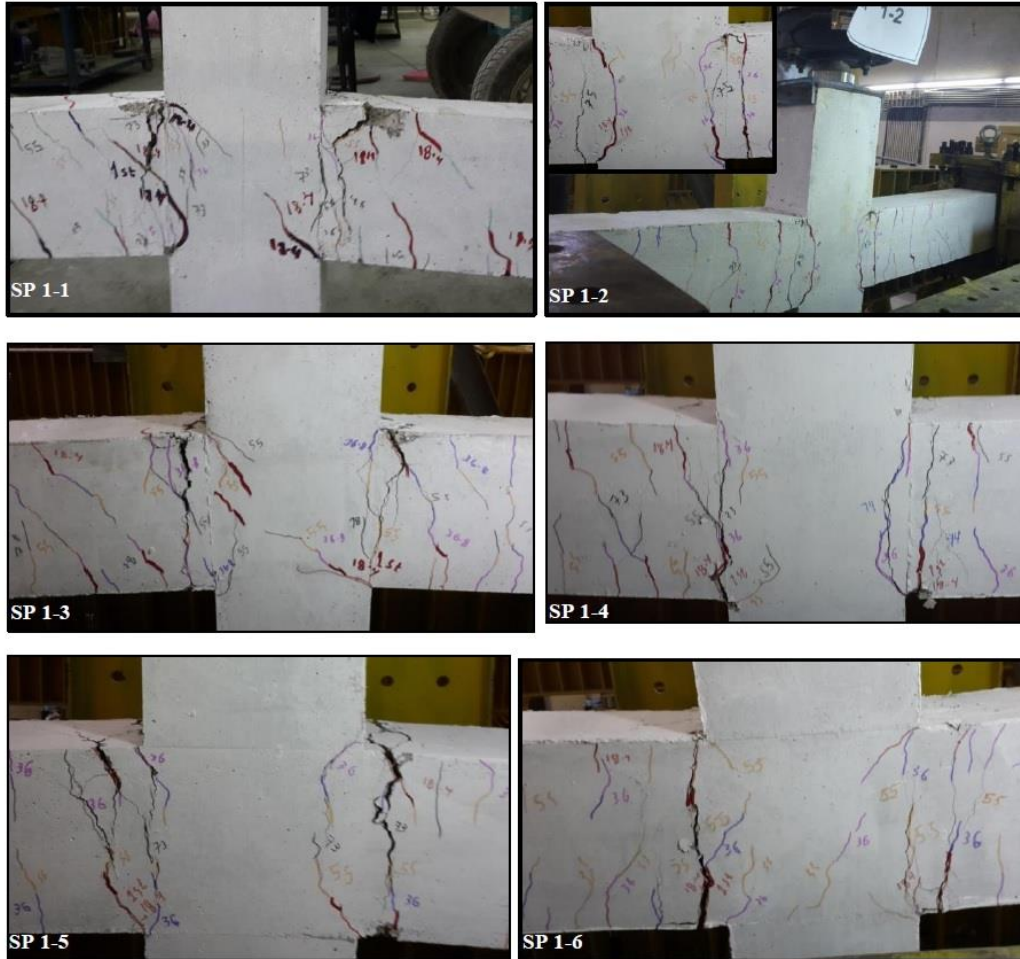


Fig. 14 The cracking pattern at failure for specimens of group (G1)

Table 5 Test results for the specimens of group (G1)

Specimen No.	No. of cycles to failure	Maximum load at failure (kN)	deflection at maximum load (mm)	Ductility factor	Cumulative energy dissipation kN-mm	Average residual displacement (mm)
SP 1-1	7(down)	73.50	30.800	2.464	4548.014	5.20
SP 1-2	9(up)	75.27	47.060	4.706	7673.111	9.20
SP 1-3	8(down)	73.07	32.610	2.964	5278.685	7.20
SP 1-4	8(down)	73.60	34.330	3.121	5691.930	7.50
SP 1-5	9(up)	73.93	53.000	4.818	7290.482	18.30
SP 1-6	6(up)	55.30	50.580	4.598	3723.926	11.20

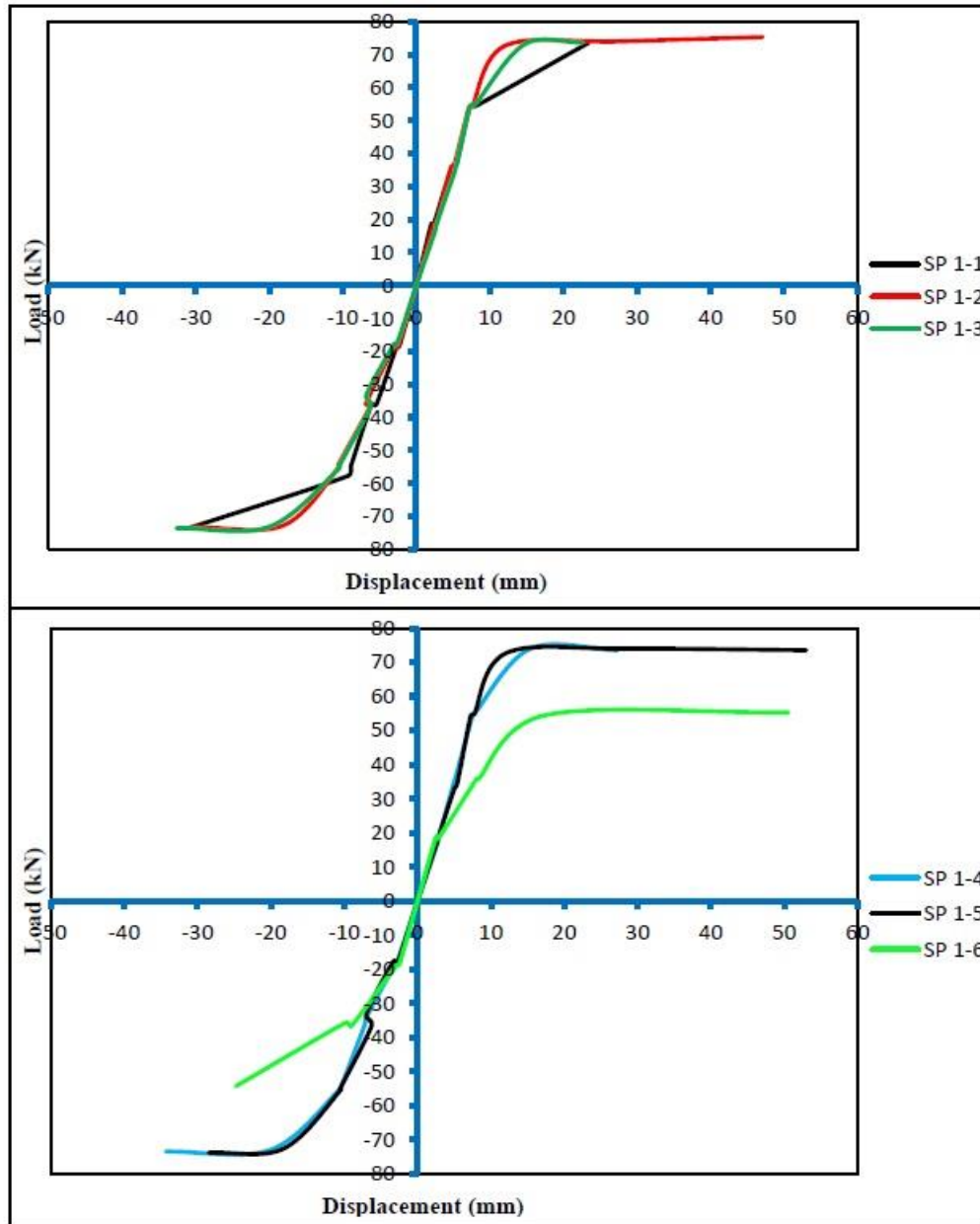


Fig. 15 Load – displacement envelope curves for specimens of group (G1)

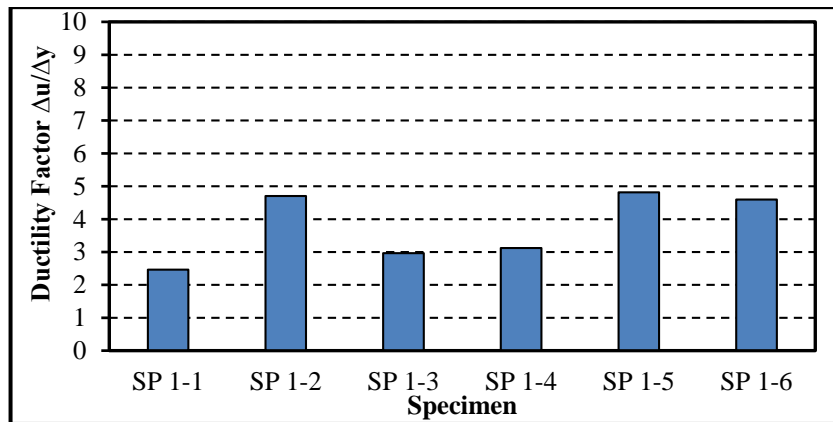


Fig. 16 The ductility factor chart for specimens of group (G1)

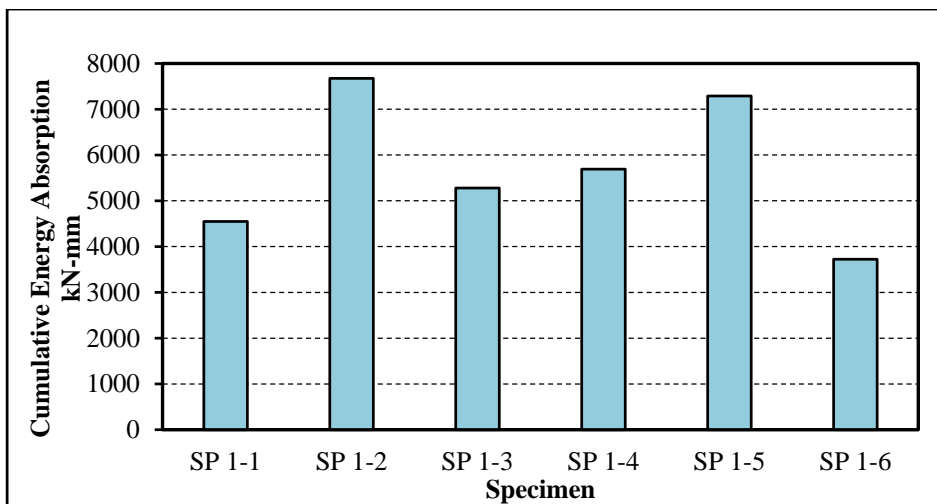


Fig. 17 The cumulative energy dissipation capacity chart for specimens of group (G1)

### 3.2.2 Group (G2)

As mentioned before, the specimens of this group are nonsymmetrical BCJs. The test results for these specimens are summarized in Table 6. Specimens SP 2-1, SP 2-2, and SP 2-3 in this group have stirrups with ( $S=S_{max}$ ) at the joint junction, while specimens SP 2-4, SP 2-5, and SP 2-6 have no stirrups. Fig. 18 shows the load-displacement hysteresis response for specimens of this group. In general, the behavior of this group is similar to that of group (G1) with a lower ductility and cumulative energy dissipation and a higher maximum load at failure.

Specimen SP2-2 show an increase in maximum failure load, ductility factor, and energy dissipation of 52.7%, 24%, and 38.8% respectively with respect to specimen SP2-1. Specimens SP2-3, SP2-4, and SP2-5 show an average increase in maximum failure load, ductility factor, and energy dissipation of 55.5%, 14.4%, and 17.8% respectively with respect to specimen SP2-1. Similar to SP1-6 in group (G1), specimen SP2-6 shows the minimum increase in maximum load at failure and

ductility factor while a decrease in energy dissipation was obtained in comparison to SP2-1 as a result of the decrease in longitudinal steel area. It is clear from the reported results for this group that the contribution of SFs is efficient in increasing the number of cycles to failure and the maximum failure load. However, the average increase in ductility factor and energy dissipation capacity is lower than that obtained in group (G1).

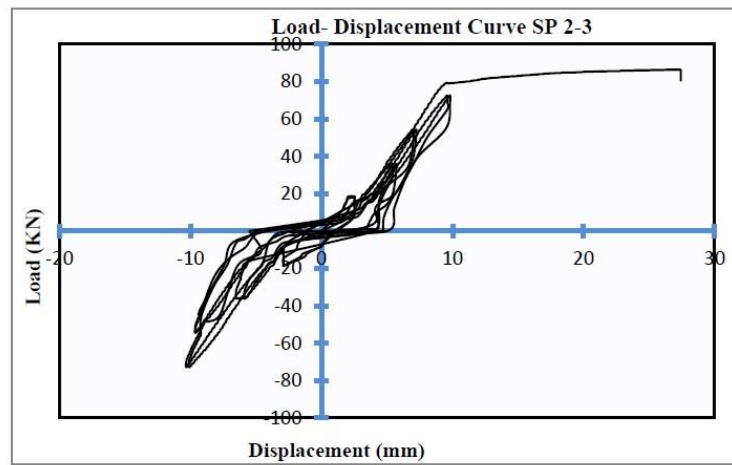
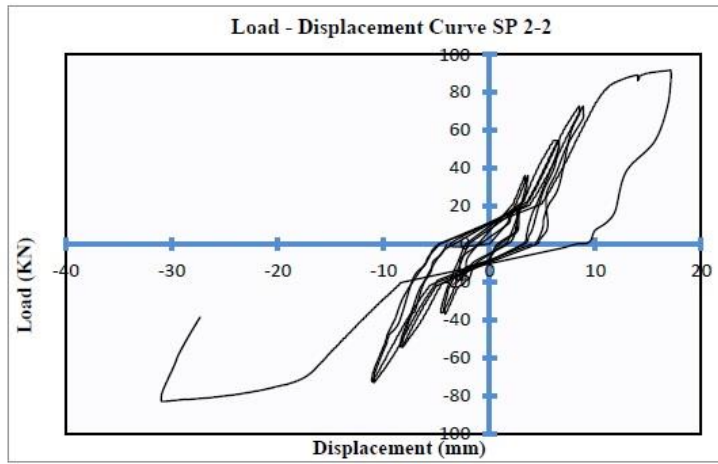
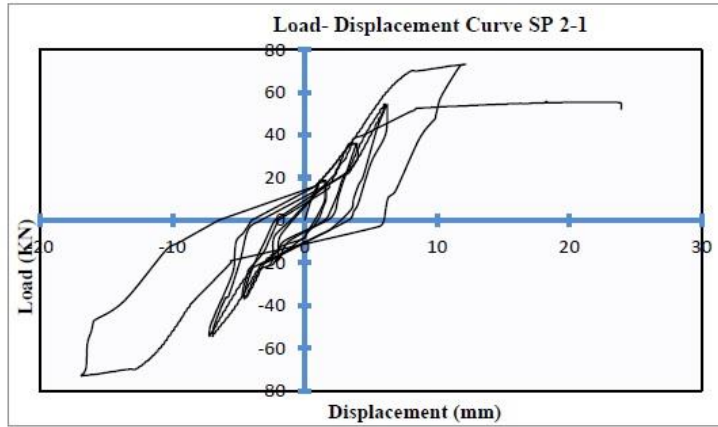
This behavior is attributed to the nonsymmetrical geometry for specimens of group (G2) in which a reduction in the shear span resulted in a brittle behavior in comparison to group (G1) specimens. The residual displacement values for this group are reported in Table 6. The average residual displacement value for this group is relatively lower when compared to group (G1) as a result of the decreased ductility in this group. Specimen SP2-2 also shows the best performance among the rest in group (G2) with respect to the maximum load at failure, ductility ratio, energy dissipation and residual displacement. In general, the addition of steel fiber in this group enhanced significantly the ductility and cumulative energy dissipation capacity. The cracking pattern at failure for specimens of this group is shown in Fig. 19. An envelope curve for each test specimen is shown in Fig. 20. The results of the ductility factor and the cumulative energy dissipation capacity for all test specimens are shown in a bar chart in Figs. 21 and 22 respectively.

It is worth to mention here that using a SFs ratio of 0.75% with  $S=S_{max}$  resulted in a decrease in ductility and energy dissipation capacity for the specimens in the two groups. This is related to the poor dispersion or agglomeration of SFs as a result of reinforcement stacking between SFs and reinforcement despite that the concrete mix itself satisfied the workability requirements. This issue should be taken into account in the selection of SFs ratio to avoid such an unpreferable behavior. Specimens with 0.5% SFs with  $S=S_{max}$  and specimens with 0.75% SFs with no stirrups show the best performance among the rest. However, a 0.5% SFs with  $S=S_{max}$  is preferred based on the reported test results.

It is also important to mention that few strength degradation is noticed for specimens in the two groups except specimen SP2-1 in which some strength degradation is observed. In fact, the failure pattern is ductile for most of the specimen which confirm that SFs increased the overall ductility of the beam-column assembly towards a more ductile failure pattern. In any case, the loading process was continued until a complete failure is obtained for all specimens.

Table 6 Test results for specimens of group (G2)

Specimen No.	No. of cycles to failure	Maximum load at failure (kN)	Deflection at maximum load (mm)	Ductility factor	Cumulative energy dissipation kN-mm	Average residual displacement (mm)
SP 2-1	8 (up)	55.00	23.580	2.620	3841.991	6.25
SP 2-2	9(down)	84.00	30.920	3.254	5333.049	7.21
SP 2-3	9 (up)	87.00	27.370	2.737	4294.776	5.25
SP 2-4	9(up)	83.50	29.890	2.846	4382.908	5.00
SP 2-5	9(down)	86.00	30.700	3.411	4894.530	8.58
SP 2-6	7(up)	62.00	26.840	3.157	2872.315	5.47



Continued-

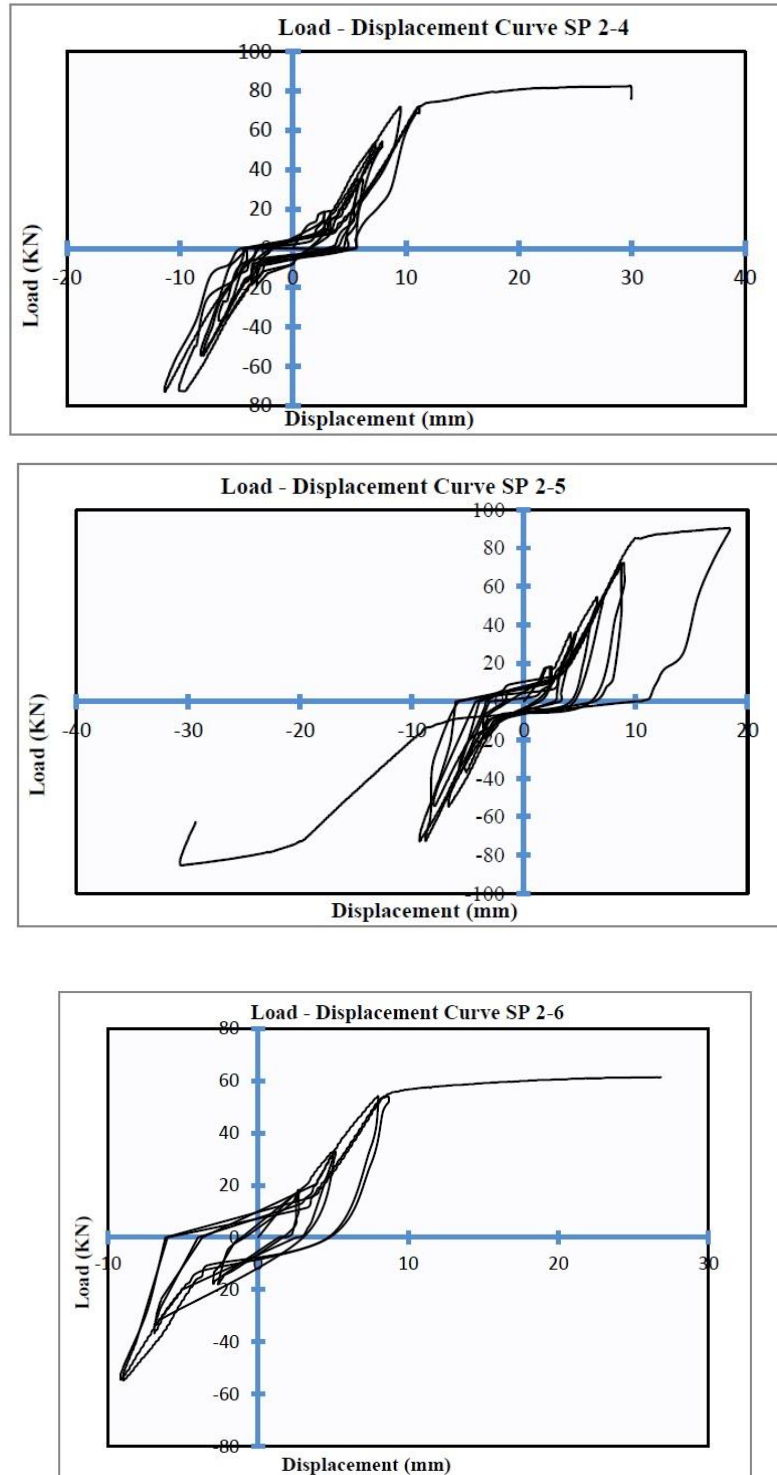


Fig.18 Load- deflection hysteresis curves of test specimens of group (G2)

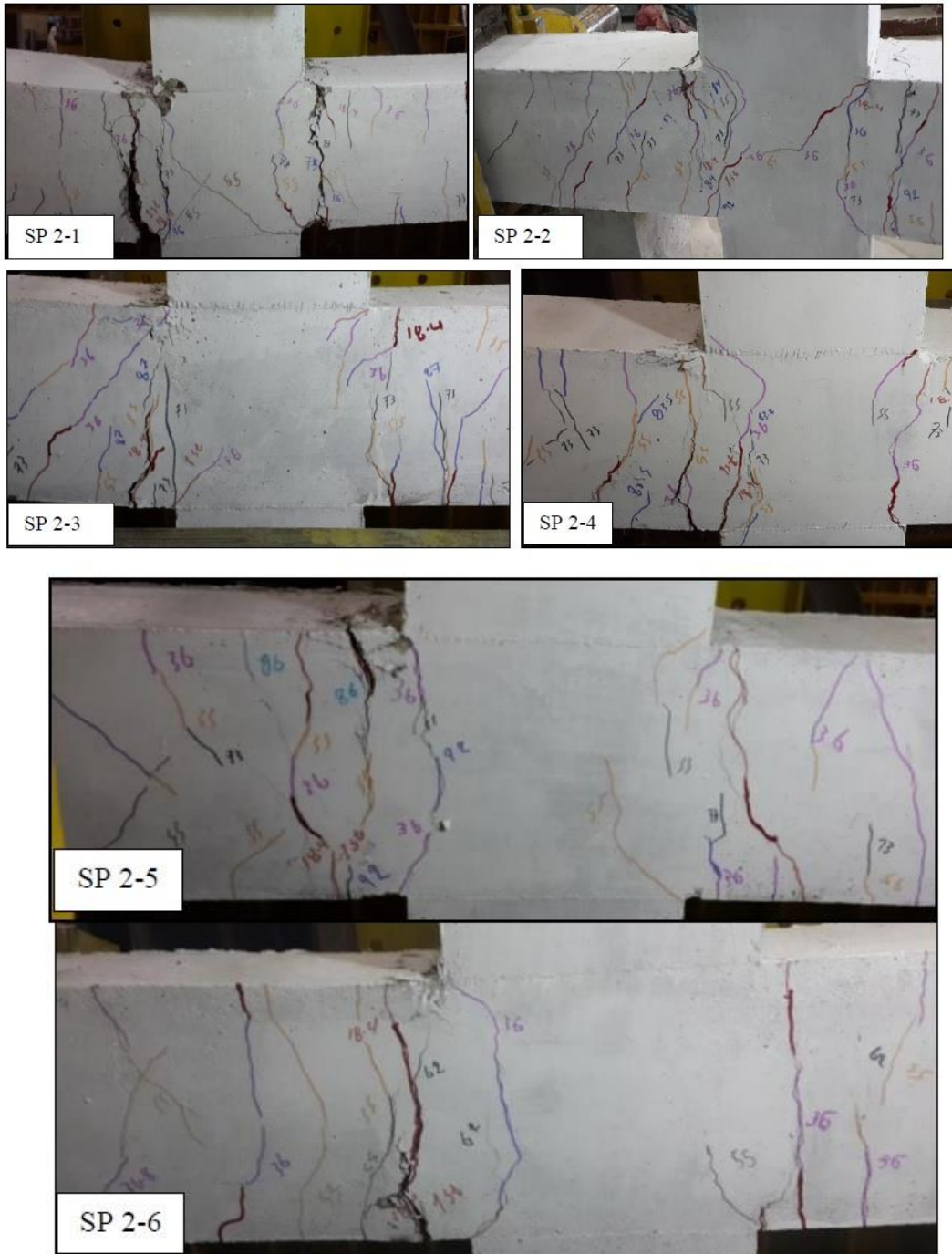


Fig. 19 The cracking pattern at failure for specimens of group (G2)

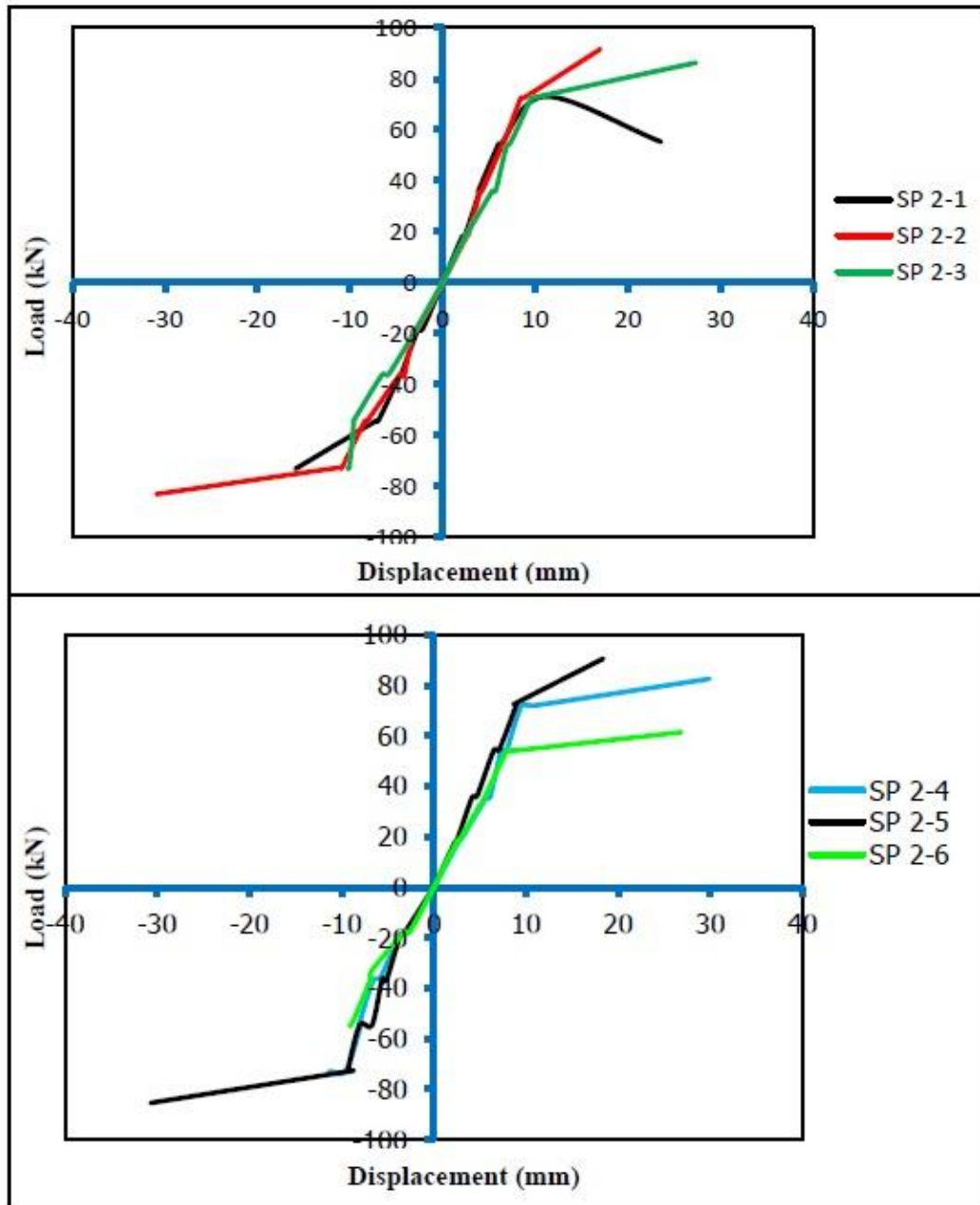


Fig. 20 Load – deflection envelope curves for the specimens of group (G2)



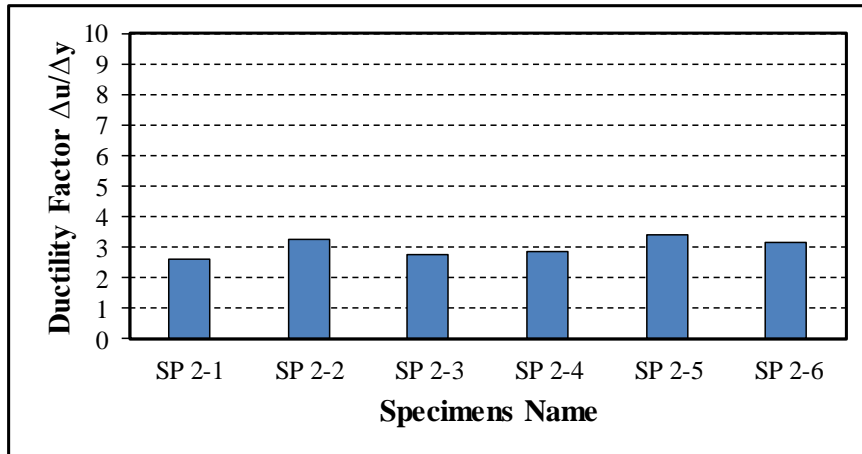


Fig. 21 The ductility factor chart for specimens of group (G2)

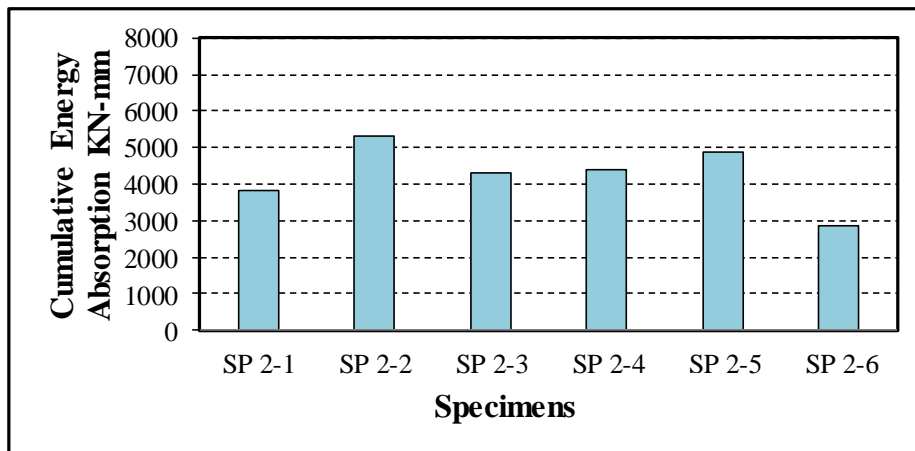


Fig. 22 The cumulative energy dissipation capacity chart for specimens of group (G2)

#### 4. Conclusions

Based on the results of the experimental program carried out for this research, the following conclusions can be drawn.

- The addition of SFs improved the mechanical properties of concrete including tensile strength, compressive strength, and flexural strength. However, these properties may be adversely affected with the addition of SFs depending on its content, water/cement ratio and the effective dispersion of SFs in the concrete mixture. The addition of 0.5% SFs resulted in an increase in

- compressive strength, tensile strength, and flexural strength of 6.2%, 23.5%, and 8.2% respectively. Using SFs ratio of 0.75% resulted in an increase of 13.2%, 33.1%, and 15.7% in compressive strength, tensile strength, and flexural strength of concrete specimens respectively.
- For specimens containing SFs ratio ( $V_f$ ) equal to (0.5%) and stirrups with a spacing ( $S=S_{max}$ ), an increase in ductility and a cumulative absorbed energy of (91%) and (68.7%) respectively for group (G1) was observed. Also, an increase in ductility and a cumulative absorbed energy of (24%) and (38.8%) respectively for the group (G2) was observed.
  - Using SFs ratio ( $V_f$ ) of (0.75%) without stirrups at joint region led to an improvement in the load-carrying capacity, ductility and cumulative absorbed energy compared to specimens with SFs ratio ( $V_f$ ) of (0.75%) and stirrups spacing ( $S=S_{max}$ ) at joint region as follows:
    - a. An increase in ductility and a cumulative absorbed energy of (96%) and (60%) respectively for the group (G1) with respect to specimen SP1-1 was observed.
    - b. An increase in ductility and a cumulative absorbed energy of (30%) and (27%) respectively for the group (G2) with respect to specimen SP2-1 was observed.
    - c. These specimens confirm the possibility of elimination of steel stirrups at joint region.
  - For specimens, containing SFs ratio ( $V_f$ ) equal to (0.75%) and stirrups spacing ( $S=S_{max}$ ) at joint region, a decrease in ductility and a cumulative absorbed energy compared to remaining specimens has been noticed. This is because of the large amount of steel which led to a poor dispersion (agglomeration) of SFs and a bond reduction between concrete and steel at the joint region which is a case that should be taken into account by the designers.

## Acknowledgements

The authors would like to thank the staff of the National Center for Construction Laboratories and Research and the Civil Engineering Laboratory of Al-Nahrain University for their support and contribution during this experimental program.

## References

- ACI 544.1R-96. (2002), State-of-the-Art Report on Fiber Reinforced Concrete.
- ACI Committee 352R-02. (2002), Recommendations for Design of Beam-Column Connections in Monolithic Reinforced Concrete Structures. Reported by Joint ACI-ASCE Committee 352.
- ASTM C 78-2002. (2002), Standard Test Method for Flexural Strength of Concrete (Using Simple Beam with Third- Point Loading). Annual Book of ASTM Standards, American Society for Testing and Materials.
- ASTM C496 / C496M-2004. (2004), Standard Test Method for Splitting Tensile Strength of Cylindrical Concrete Specimens. ASTM International, West Conshohocken, PA.
- B.S. 1881 (1989), Method for determination of compressive strength of concrete cubes. British Standards Institution, Part 116.
- Banthia, N., Yan, C. and Bindiganavile, V. (2000), "Development and application of high-performance hybrid fiber-reinforced concrete", *Proceedings of the 5th RILEM International Symposium on Fiber-Reinforced Concrete BEFIB*, RILEM Bagnaux, France.
- British Standards Institution, BS 5328 (1997), "Methods for specifying concrete mixes", Issue 2.
- Ganesh, K.D. and Prabavathy, S. (2015), "Experimental study on seismic performance in beam-column joint using hybrid fibers", *Int. J. Sci. Eng. Appl.*, **4**(3), 134-137.
- Kang, S.B. and Tan, K.H. (2015), "Behaviour of precast concrete beam-column sub-assemblages subject to column removal", *Eng. Struct.*, **93**, 85-96.
- Keerthana, J.D. and Reddy, C.S. (2014), "Experimental investigation on hybrid steel fiber reinforced concrete

- beam– column joints under cyclic loading”, *IJRST*, **1**, 6-11.
- Kim, J. and LaFave, J.M. (2009), “Joint shear behavior of reinforced concrete beam-column connections subjected to seismic lateral loading”, NSEL Report Series Report No. NSEL-020, Department of Civil and Environmental Engineering, the University of Illinois at Urbana-Champaign.
- Kumar, S. (1988), “A Study of Reinforced Concrete Beam-Column Joints under Uni-Axial Bending”, M. Tech, Dissertation, Inst. Of Technology, Benara Hindu University, Varanasi.
- Kumar, V., Nautiyalil, B.D. and Kumar, S. (1991), “A study of exterior beam-column joints”, *The Concrete J.*, **65**, 2821-2836.
- Liang, X.W., Wang, Y.J., Tao, Y. and Deng, M.K. (2016), “Seismic performance of fiber-reinforced concrete interior beam-column joints”, *Eng. Struct.*, **126**, 432-445.
- Moehle, J.P., Hooper, J.D. and Lubke, C.D. (2008), “Seismic design of reinforced concrete special moment frames: A guide for practicing engineers”, US Department of Commerce.
- Nguyen, X.H., Le, D.D., Nguyen, Q.H. and Nguyen, H.Q. (2020), “Seismic performance of RCS beam-column joints using fiber reinforced concrete”, *Earthq. Struct.*, **18**(5), 599-607.
- Nimse, R.B., Joshi, D.D. and Patel, P.V. (2014), “Behavior of wet precast beam- column connections under progressive collapse scenario: an experimental study”, *IJASE*, **6**, 149-159.
- Oinam, R.M., Kumar, P.C.A. and Sahoo, D.R. (2019), “Cyclic performance of steel fiber-reinforced concrete exterior beam-column joints”, *Earthq. Struct.*, **16**(5), 533-546.
- Paulay, T., Park, R. and Priestey, M.J.N. (1978), “Reinforced concrete beam-column joints under seismic actions”, *ACI J.*, **75**, 585-593.
- Qi, J., Wang, J. and Feng, Y. (2019), “Shear performance of an innovative UHPFRC deck of composite bridge with coarse aggregate”, *Adv. Concrete Constr.*, **7**(4), 219-229. <https://doi.org/10.12989/acc.2019.7.4.219>.
- Romanbabu, M.O., Choudhury, A.M. and Laskar, A.I. (2013), “Experimental study on beam- column joint with fibers under cyclic loading”, *IOSR Journal of Engineering*, **3**, 13-23.
- Sara, M., Abbas, A. and Masoud, S. (2015), “Behavior of interior RC wide and conventional beam-column roof joints under cyclic load”, Structural Engineering Division, Faculty of Civil and Environmental Engineering, Tarbiat Modares University, Tehran, Iran.
- Sarmiento, P.A., Torres, B., Ruiz, D.M., Alvarado, Y.A., Gasch, I. and Machuca, A.F. (2019), “Cyclic behavior of ultra-high performance fiber reinforced concrete beam-column joint”, *Struct. Concrete*, **20**(1), 348-360.
- SikaViscoCrete -5930. (2010), Product data sheet. Edition 6, 2010. Version no. 01.10
- Sohailuddin, S.S. and Shaikh, M.G. (2013), “Finite element modeling of reinforced concrete beam column joint using ANSYS”, *Int. J. Struct. Civ. Eng. Res.*, **2**, 22-31.
- Sorelli, L.G. (2003), Some Studies on the Assessment of the Toughness of Steel Fiber Reinforced Concrete with Emphasis on Hybrid Fiber Systems. Ph.D., Department of Civil Engineering of the University of Brescia, Brescia, Italy.
- Sorelli, L.G., Meda, A. and Plizzari, G.A. (2005), “Bending and uniaxial tensile tests on concrete reinforced with hybrid steel fibers”, *J. Mater. Civ. Eng.*, **17**, 519-527.
- Sorelli, L.G., Meda, A. and Plizzari, G.A. (2006), “Steel fiber concrete slabs on ground: A structural matter”, *ACI Struct. J.*, **103**, 551-558.
- UFC 4-023-03 DoD (2016), “Design of buildings to resist progressive collapse. USA, <http://dod.wbdg.org/>.
- Xilin, L., Tonny, H., Urukup, Sen Li and Fangshu Lin (2012), “Seismic behavior of interior RC beam-column joints with additional bars under cyclic loading”, *Earthq. Struct.*, **3**(1), 37-57.
- Zhou, H. and Zhang, J. (2014), “Interaction of internal forces of interior beam-column joints of reinforced concrete frames under seismic action”, *Struct. Eng. Mech.*, **52**(2), 427-443.